New model to study the outdoor degradation of thin–film photovoltaic modules

Michel Piliougine[a,*], Paula Sánchez-Friera[b], Giovanni Petrone[a], Francisco José Sánchez-Pacheco[c], Giovanni Spagnuolo[a] and Mariano Sidrach-de-Cardona[d]

[a]*Dipartimento di Ingegneria dell'Informazione ed Elettrica e Matematica Applicata. Università degli Studi di Salerno. 84084 Fisciano (SA), Italy*
[b]*Solar PV Consultancy Services, Solkeys. 33204 Gijón, Spain*
[c]*Departamento de Tecnología Electrónica – Universidad de Málaga. 29071 Málaga, Spain*
[d]*Departamento de Física Aplicada II – Universidad de Málaga. 29071 Málaga, Spain*

ABSTRACT

The performance of four thin-film photovoltaic modules is analyzed after an initial stabilization period and a subsequent outdoor exposition. The seasonal variations and the degradation rates of a single-junction hydrogenated amorphous silicon (a-Si:H) module, a tandem amorphous microcrystalline Silicon (a-Si/μc-Si) module, a heterostructure cadmium sulfide-cadmium telluride (CdS/CdTe) module and a copper indium gallium selenide (CIGS) are examined and correlated to spectral changes. The *I-V* curves have been measured every five minutes; the electrical parameters and parasitic resistances have been identified. By exploiting a number of experimental measurements acquired within a narrow interval of irradiance and cell temperature, a novel mathematical model has been developed and fitted: it considers a stationary seasonal variation component and a linear long-term degradation component. The results show annual power degradation rates of 4.0% for the a-Si:H module, 3.4% for the a-Si/μc-Si and 3.5% for the CdS/CdTe, whereas for the CIGS module the annual degradation is not significant, i.e. 0.2%.

Keywords: amorphous silicon, cadmium telluride, copper indium gallium selenide, microcrystalline silicon, photovoltaic degradation, thin film.

*Corresponding author
Email addresses: mpiliouginerocha@unisa.it (M. Piliougine); paula@solkeys.com (P. Sánchez-Friera); gpetrone@unisa.it (G. Petrone); fsanchezp@uma.es (F.J. Sánchez-Pacheco); gspagnuolo@unisa.it (G. Spagnuolo); msidrach@uma.es (M. Sidrach-de-Cardona)

1. Introduction

Thin–film PV modules had an important presence in the global market a decade ago, reaching about 17% of the global production in 2009 [1] and then gradually loosing share due mostly to the improvements and cost reduction of the crystalline silicon (c–Si) technologies. Nevertheless, they still constitute today a viable option, which is particularly attractive in certain applications with a large growth potential such as building integrated photovoltaics [2, 3]. The market share of thin–film technologies in the global PV market is expected to be limited. Nevertheless, understanding the degradation mechanisms of a-Si and micromorph modules could provide insights on the behaviour of high efficient silicon hetero–junction technologies, which also contain a-Si layers, and are recently attracting a lot of interest.

The degradation mechanisms associated to thin–film modules have been the subject of many works for the last years, e.g. [4–26], although less than those ones affording the degradation of c–Si modules [27]. Thin–film PV module degradation rates are in general higher, and with wider dispersion than their crystalline counterparts [28], this being one of the factors that have hampered the market growth of these modules. However, some reports [29, 30] have stated the that thin–film technologies may have better stability. In any case, it is highly desirable to conduct further studies to gain a deeper insight into the degradation of thin–film modules. This will contribute to improve their reliability and reduce uncertainties in the estimation of their long–term energy production in real systems.

Table 1 summarizes some thin–film module degradation rates. Even for the same technology, there is a significant dispersion of the levels of degradation. Considering a–Si:H, many papers report annual degradation rates around 2% [12, 14, 18, 19] or even lower [6, 16, 20], but other studies report rates ranging between 5 and 7% [4, 17]. Lower degradation rates are obtained for modules based on tandem cells of amorphous and microcrystalline silicon (a–Si/μc–Si), lying in the range from 1.5 to 2.2% [8–11, 13], although higher rates, between 2.7 and 3.9%, are reported in [15].

The dispersion of the degradation rates for Cadmium Telluride (CdTe) is even higher. Whereas some authors [21, 26] show very low degradation rates, i.e around 0.6%/year, some works evidence rates between 1.4% and 10% [4, 5, 7, 10, 11, 14, 16, 18, 19]. Regarding CI(G)S technologies, a wide difference in the results documented by different authors is evident [9, 11, 14, 16, 20, 22, 31], with annual degradation rates ranging from 0.2 to 2.6%. In general, significantly lower rates are reported in comparison to the other thin–film technologies with a few exceptions [18, 24]. The large dispersion found in reported degradation rates is partly due to the difficulties associated to ensure a reliable measurement of thin–film PV modules variables [32]. In round robin measurements conducted by different test laboratories, divergences between 3 and 6% were found for thin–film PV modules, whereas for crystalline silicon modules, divergences were under 1% for the same laboratories. In general, it is known that the output of a thin–film module depends on its actual operating conditions, but it is also affected by its past history, both in terms of temperature and irradiance [33], that may affect their performance permanently or reversibly.

The initial stabilization period of the modules is normally observed in all thin–film PV technologies. As for the a–Si based technologies, the well–known Staebler-Wronski effect [34] leads to about 20% of the initial efficiency drop during the first weeks of exposure to sunlight due to the formation of meta–stable defects in the a–Si:H semiconductor. The phenomenon depends on the level of irradiation and also on the device temperature [35]. In fact, the initial performance can be recovered by annealing above certain value of temperature, i.e. from $\approx$ 130 °C. For lower temperature levels there is a partial recovery depending on the thermal history of the device and on the climate conditions. The stabilization period for a–Si is typically considered to be of about 6 weeks [36–39], during which the most significant power decay takes place. Other studies report longer periods for a complete stabilization [13, 40, 41]. Other thin–film modules suffer a strong initial degradation due to light exposure. For CdTe, 6–week stabilization period is commonly accepted. Del Cueto et al. [42] state an initial drop after the first 400-600 hours of sun exposure, which is equivalent to 6-8 weeks. Deline et al. [43] recommend an initial period of 120 KWh/m^2, which is equivalent to 6 weeks assuming a minimum daily irradiation of 2.78 kWh/m^2, estimated for our site (Málaga, Spain) in the worst–case month [44]. Regarding CIGS, there is not agreement in the literature [45]. Some works show a stable performance since the first use [14]; others conclude that at least 1 year is necessary to reach a stable behavior [46].

Despite its importance, not all the studies state if the initial stabilization period is included or not in the reported degradation rates. For example, in Demirtaş et al. [47] the degradation rate is estimated during the first year of operation for two CdTe and CIS arrays, by obtaining 22% and 32% respectively. These very high values suggest that the initial drop is included in the degradation rate, which would not be representative of a long–term study.

Date	Reference	Technology	Brand/model/identification	Years	Load†	$-\%P_{\max}$/year
2021	Cassini et al. [4]	a–Si:H	Module 3*	15	inverter	5.5
		CdTe	Module 4*	7	inverter	5.6
2021	Kumar et al. [5]	CdTe	Specimen CdTe-6*	1	ND	1.37
2020	Singh et al. [6]	a–Si:H	same brand/model, a-Si_1*	3	ND	1.32
			same brand/model, a-Si_2*	3	ND	1.12
			same brand/model, a-Si_3*	3	ND	1.04
2018	Kichou et al. [7]	CdTe	Calyxo/CX3-80	2	MPP	5.55
2018	Aarich et al. [8]	a–Si/μc–Si	Array series/parallel*	+2.5	inverter	1.5
2017	Limmanee et al. [9]	a–Si/μc–Si	Thin Si 1*	4	inverter	2.1
		a–Si/μc–Si	Thin Si 2*	4	inverter	1.8
		CI(G)S	CIGS*	4	inverter	1.7
2017	Ozden et al. [10]	a–Si/μc–Si	Kaneka/U-EA105	4	inverter	1.88
		CdTe	Abound/AB1-67B	4	inverter	10.6
2017	Tahri et al. [11]	a–Si/μc–Si	Sharp/NA-121	3	ND	1.73
		CI(G)S	Solar Frontier/SF150-S	3	ND	2.34
2016	Kichou et al. [12]	a–Si:H	Array series/parallel*	3.5	inverter	2.30
2016	Kichou et al. [13]	a–Si/μc–Si	Array series/parallel*	3.5	inverter	2.20
2016	Silvestre et al. [14]	a–Si:H	Kaneka/G-EA60	5	ND	2.28
		a–Si/μc–Si	Sharp/NA-121	5	ND	2.72
		CdTe	Fist Solar FS-270	5	ND	4.55
		CI(G)S	Shell Powermax Ultra80C	5	ND	1.04
2015	Ferrada et al. [15]	a–Si/μc–Si	Array series/parallel*	$\approx$1.5	inverter	2.7$\sim$3.9
2015	Kyprianou et al. [16]	a–Si:H	Mitsubishi/MA100T2	8	inverter	1.38
		CdTe	Fist Solar FS-60	8	inverter	1.96
		CI(G)S	Würth Solar/WS11007-75	8	inverter	2.33
2014	Sharma et al. [17]	a–Si:H	Array series/parallel*	+2	inverter	6.4
2014	Ye et al. [18]	a–Si:H	Specimen 6*	3	MPP	$\approx$ 2
		CI(G)S	Specimen 9*	3	MPP	$\approx$ 6
		CdTe	Specimen 10*	3	MPP	$\approx$ 2
2014	Makrides et al. [19]	a–Si:H	Mitsubishi/MA100T2	5	inverter	1.87
		CdTe	First Solar/FS-60	5	inverter	2.27
		CI(G)S	Würth Solar/WS11007-75	5	inverter	1.95
2013	Gottschalg et al. [20]	a–Si:H	Specimen a–Si–1*	+4	ND	1.26
		CI(G)S	Specimen CIGS–1*	5.5	ND	2.74
		CI(G)S	Specimen CIGS–2*	5.5	ND	0.42
2012	Strevel et al. [21]	CdTe	Solar Cells Inc. (act. First Solar)	17	inverter	0.53
2011	Jordan and Kurtz [22]	CI(G)S	ShellSolar/PowerMax Eclipse 80-C	+5	inverter	$\leq$ 0.32
2008	Del Cueto et al. [23]	CI(G)S	Specimens 1988:A*	+17	resistor	0.90
		CI(G)S	Specimens 1990:A*	16.5	resistor	0.21,0.32
		CI(G)S	Specimens 1992:A*	15.5	resistor	0.43
		CI(G)S	Specimens 1994:A*	13	resistor	0.95,1.08
		CI(G)S	Specimens 1997:A*	10	resistor	1.27,1.35,2.10
		CI(G)S	Specimens 1997:A*	10	resistor	2.10
		CI(G)S	Specimens 1998:A*	+9	resistor	2.25
		CI(G)S	Specimens 1997:A*	6	resistor	1.27,1.35
		CI(G)S	Specimens 2002:B*	5.5	resistor	0.89,1.80
		CI(G)S	Specimens 2002:B*	+4	resistor	0.65
		CI(G)S	Specimens 1998:A*	4	resistor	2.14
		CI(G)S	Specimens 2004:A*	3	resistor	2.6,2.9,3.8,4.7
2006	Durisch et al. [24]	CI(G)S	Siemens/ST40	1	ND	8.4,9.5
2005	Adelstein and Sekulic [25]	a–Si:H	Array series/parallel*	1	inverter	7.3
			*(same installation, following years)**	5	inverter	1.7
2001	Marion et al. [26]	CdTe	Solar Cells Inc. (act. First Solar)	4	inverter	0.6

* The actual brand/model are not defined in the referenced paper

† It specifies if the modules are normally (when they are not being measured): "resistor" (with a fixed resistor), "MPP" (at its maximum power point with an optimizer circuit), "inverter" (several of them connected as an array to a grid inverter), or "ND" (not defined in the referenced paper).

Table 1
Summary of different studies of degradation for thin–film modules.

Another frequent issue in thin–film PV degradation analyzes is related to the accuracy of the measurements. It is not uncommon to find studies [48] based on measurements performed by *I–V* portable curve tracers, which are designed to characterize whole strings. Unfortunately, they offer an insufficient accuracy to specify the level of degradation of an individual module, especially if the exposure period is short: the actual degradation is often smaller than the measurement error. Moreover, as many of these devices are based on a capacitive load, they are not fast enough to accurately sample the *I–V* curve in proximity of the short–circuit current, thus further reducing the accuracy of the I_{SC} and R_{Sh} estimations. A too fast acquisition of the *I–V* curve, as it happens with some solar simulators, may lead to transient effects (e.g. the direction of the voltage sweep changes the shape of the curve), with consequent errors in the estimation of P_{max}, in particular when measurements concern high capacitance thin–film technologies [49].

Outdoor measurements are usually translated to Standard Test Conditions (STC) by using correction procedures. The latter ones introduce additional uncertainties in the final values, which can be sometimes larger than the determined degradation rates. For example, the procedures 1, 2 and 4, described in the IEC 60891:2021 [50], as most of other methods in the literature, require, in addition of the temperature coefficients, other internal parameters that are hard to be obtained and whose values are usually affected by a significant approximation. The introduced uncertainty can be especially large in climates where it is not possible to reach high irradiance values, e.g. close to 1 000 W/m^2, with low cell temperatures, so that the temperature gap to correct (e.g. from 50 °C to 25 °C) is very large.

As a further element affecting degradation analyzes based on outdoor measurements, variations of the spectrum have to be accounted for. Some thin–film technologies show a narrow spectral response, which leads to significant performance changes due to spectral variations throughout the year. For example, in King et al. [41] it is stated that the energy production of an a–Si module could increase even by a 2% in summer with respect to its output under AM1.5, with a decrease of a 5% in winter. As a result, a valid study of thin–film degradation at outdoor conditions should consider measurements performed under a similar spectrum, e.g., acquired during the same month of different years.

In this work, the results achieved by applying a rigorous procedure to analyze the evolution of the outdoor performance of four different types of thin–film modules are presented. The modules are of the following technologies: single-junction hydrogenated amorphous silicon (a–Si:H), tandem of amorphous and microcrystalline silicon (a–Si/μc–Si), heterostructure of cadmium sulfide and cadmium telluride (CdS/CdTe) and copper indium gallium selenide (CIGS). The modules under study were installed on the roof of the *Photovoltaic Laboratory* of the *University of Málaga* in the South of Spain and they have been monitored during a period of around 20 months, after *a stabilization period of 8 weeks*. The reported degradation rates quantify the evolution of these indicators: the maximum power (P_{max}), the short–circuit current (I_{SC}), the open–circuit voltage (V_{OC}), the current at the MPP (I_{max}), the voltage at the MPP (V_{max}), the fill factor (FF), the series resistance (R_S), and the shunt resistance (R_{Sh}), these last two referred to the single diode model (SDM) [51].

Aimed at distinguishing between the seasonal annual variations and the long–term degradation of the previous indicators, *a novel methodology is proposed*, based on fitting the measured data to a non–linear model that can deal with non–equispaced data and with missing information. This model assumes that the amplitude of the seasonal trend is a percentage of a base value, which in turn degrades over time. The fitting parameters obtained will be used to estimate the annual degradation rates and correlate the behavior of the modules to the spectral variations.

The paper is organized as follows: In Section 2, the methodology employed for the measurement and parameters extraction is described. The results of the evolution of the electrical parameters and parasitic resistances are presented in Section 3. Sections from 3.1 to 3.4 analyze the obtained results for each technology, contrasting them with previous literature. Finally, Section 4 summarizes the main conclusions of this work.

2. Methodology

2.1. Description of PV modules

One specimen for each technology has been used, labelled as M1, M2, M3, and M4. The main specifications of the modules under study are summarized in Table 2. M1 and M2 are based on amorphous silicon, one of the most sustainable PV technologies, due to its abundance, low temperature coefficients, small amount of raw material required and low–energy manufacturing process [52]. Amorphous silicon is usually hydrogenated, as the incorporation of atomic hydrogen passivates the dangling bonds typical of the amorphous structure thus improving the cell efficiency. The

Module	M1:a-Si		M2:a-Si/μc-Si		M3:CdTe/CdS		M4:CIGS	
Manufacturer	Kaneka[53]		PhoenixSolar[54]		FirstSolar[55]		Solyndra[56, 57]	
Model	GEA–060		PHX–120–LV		FS–272		SL-001-157C	
Number of cells	108		96		116		150	
Efficiency [%]	6.3		8.51		10.07		7.99	
Temperature coefficient α [%/°C]	+0.075		+0.07		+0.04		−0.06	
Temperature coefficient β [%/°C]	−0.305		−0.30		−0.25		−0.38	
Temperature coefficient γ [%/°C]	−0.23		−0.24		−0.25		−0.35	
NOCT [°C]	–		44		45		45	
Electrical Parameters*	STC	NOCT	STC	NOCT	STC	NOCT	STC	NOCT
Short–circuit current I_{SC} [A]	1.19	–	3.34	2.70	1.23	1.01	2.54	1.95
Open–circuit voltage V_{OC} [V]	92	–	59.20	55.10	88.7	82.5	97.60	88.30
Maximum power P_{max} [W]	60	–	121.0	91.80	72.5	54.4	157.0	113.4
Current at maximum power I_{max} [A]	0.90	–	2.69	2.19	1.09	0.87	2.20	1.69
Voltage at maximum power V_{max} [V]	67	–	45.00	41.90	66.6	62.4	72.30	67.10

* STC: $G = 1\,000$ W/m^2, $T_{cell} = 25$ °C, AM1.5 — NOCT: $G = 800$ W/m^2, $T_{air} = 20$ °C, $Wind_{speed}$=1 m/s, AM1.5

Table 2
Specifications of the photovoltaic modules under study.

hydrogenated amorphous silicon (a–Si:H) material has a high direct band gap of 1.7 eV which leads to high absorption in the short wavelengths. M1 is a single–junction a–Si:H module by *Kaneka* with a p-i-n cell configuration and a nameplate stabilized efficiency of 6.3% [53]. M2 is a tandem a-Si/μc-Si module by *Phoenix Solar* which includes a top a–Si cell and a bottom μc–Si cell, and has a efficiency of 8.5% [54]. Both M1 and M2 have power tolerances of +10%/−5% and power warranties of 80% at 25 years. They were built with a glass–foil superstrate configuration. The *Kaneka* module includes a 5 mm float glass whereas the *Phoenix Solar* module is built over a 4 mm low–iron front glass. Both have EVA as encapsulant, a fluorine–based foil backsheet and aluminum frames.

M3 is a CdS/CdTe module by *First Solar* with a nameplate efficiency of 10.07% and a power tolerance according to the manufacturer of ±5%. It is a double–glass frameless module, with glass panes of 3.2 mm thickness, heat strengthened at the front and tempered at the back, laminated with an encapsulant and an edge seal [55]. M4 is a CIGS module, material that has a very high absorption coefficient and also a large direct band gap. Manufactured by *Solyndra*, with a total area nameplate efficiency of 7.99% and a power tolerance of ±4% [56]. This module has a special construction which was conceived to improve generation at low incidence angles. It is built from a series of tubes, which are composed of two cylinders one inside the other. The CIGS cell is deposited over the internal cylinder and optically coupled to the outer cylinder. The tubes are hermetically sealed with metal caps at the ends of the tubes.

2.2. Experimental set–up

The modules were mounted on a fixed open–rack structure facing to south with an inclination of 21°. The installation is in Málaga (latitude 36.7 N, longitude 4.5 W, altitude 50 m) in the south of Spain, very close to the Mediterranean Sea and with typical meteorological conditions of 1 890 kWh/m^2 of annual horizontal global irradiation, average daytime ambient temperature of 18 °C, relative humidity of 63% and wind speed of 1 m/s.

The meteorological variables were acquired by a weather station composed of an anemometer and a wind vane (Young 03002L), a combined sensor of air temperature and relative humidity (Young 41382LC) and two irradiance sensors on the module plane: a thermo–electric pyranometer Kipp & Zonen CM–21 [58] and a reference cell from the manufacturer Atersa [59]. Whereas the former provides the irradiance used as reference value, the latter fast–response sensor is only used to discard those *I–V* curves measured under changing conditions of irradiance.

The cell temperature is monitored with the use of Pt100 Resistance Temperature Detectors (RTD) using a four–wire connection to avoid ohmic losses. These sensors are encapsulated by a silicone sheath allowing a better coupling to the back surface of the PV modules [60]. Several sensors are used for each module and an average cell temperature is calculated, following the schema depicted in IEC 60891:2021 [50], to take into account edge effects.

The spectrum of the solar irradiance is also monitored using a spectroradiometer EKO MS–710 installed on the module plane, covering from 350 to 1100 nm. Although this range could not be enough for all the technologies under study (e.g. a–Si: 300–790 nm or CIGS: 370–1240 nm [61]), the solar spectrum for the portions not covered is almost insignificant for our purposes (the irradiance between 300–350 nm and 1100–1240 nm are only 1.3% and 4.9% of the total solar irradiance [62] respectively).

The output signals of all the sensors are connected to a Compact FieldPoint™ cFP–2120 controller and acquisition system from National Instruments [63]. The system is connected to the local Ethernet in such a way any computer can retrieve the measurements in real time. The *I–V* curve acquisition system was described in a previous paper [64]. A four–quadrant power supply performs the voltage sweep at the PV module terminals in a suitable voltage range. The *I–V* samples are acquired by a pair of multimeters triggered by a common square signal to ensure the simultaneity of both readings. The acquired *I–V* curves are stored in a relational database and can be downloaded and exported for further treatment through a web application [65]. The *I–V* acquisition time and the number of points can be configured, setting these parameters to 1 second and 100 points respectively. In order to share the equipment between all the installed PV modules, a relay box is used to select automatically the specimen to be measured, in such a way all of them are measured in sequence every 5 minutes. The PV modules have remained at open–circuit condition when they were not measured.

A detailed analysis of the uncertainties of this measurement system, used in Málaga for the last years, is provided in [66]. The short–circuit current I_{SC} is estimated with an expanded uncertainty of 0.8% whereas the expanded uncertainty for the open–circuit voltage V_{OC} is 0.5%. However, the estimations of P_{max}, V_{max} and P_{max} have expanded uncertainties of 1.1% (coverage factor $k = 2$ in all the cases accordingly to ISO/IEC Guide 98-3 [67]). Finally, the expanded uncertainty for the calculated values of FF, R_S and R_{Sh} are 1.6%, 3% and 7% respectively.

2.3. Measuring and data extraction procedure

Before the start of the measuring campaign, the modules were stabilized by leaving them outdoors *for an initial period of 8 weeks*. During this stabilization period the PV modules have been also at open–circuit condition without any load connected to them. As it has been stated in Section 1, the purpose of this period is to avoid the strong power drop during the first weeks of exposure, assuming that the complete stabilization period could take much more time.

After stabilization, the *I–V* curves of the modules have been measured at 5–minute intervals during the sun hours for the whole period under assessment, that lasts around 20 months. Simultaneously with the *I–V* curve, the following magnitudes were measured: irradiance on the module plane, ambient temperature, cell temperature (at several points), speed and direction of the wind, relative humidity and solar irradiance spectrum. All the modules and the sensors were regularly cleaned to avoid soiling.

The estimation of the electrical parameters from the discrete points of the *I–V* curves is done following the indications given by Emery [68]. Once the main electrical parameters have been estimated, a parameter identification method based on the single–diode model can be applied to estimate the values of the series and shunt resistances, such as the one described by Toledo and Blanes [69]. This analytical method requires the coordinates and the derivatives of four points of the *I–V* curve; therefore, I_{SC}, V_{OC}, P_{max}, and an additional point, selected by means of the $\alpha-$power function described in the same paper, have been used. A value of $\alpha = 10$, thus giving a point between the MPP and the open–circuit point, has been settled.

In addition, from the measurements of the solar spectrum, the associated *average photon energy* (APE) values were computed. The APE is defined as the mean energy value (expressed in eV) of the photons from a given spectral distribution [70] and it is used to be estimated referred to a finite wavelength interval $[\lambda_a, \lambda_b]$ as:

$$\mathrm{APE}_{\lambda_a}^{\lambda_b} = \frac{\int_{\lambda_a}^{\lambda_b} G_\lambda(\lambda) d\lambda}{\int_{\lambda_a}^{\lambda_b} \frac{G_\lambda(\lambda)}{\epsilon_\lambda} d\lambda} \tag{1}$$

where G_λ is the spectral irradiance on the module plane for a specific wavelength λ (in $\mathrm{Wm^{-2}/nm}$) and ϵ_λ is the energy (in eV) of a photon of wavelength equal to λ. This APE indicator is a useful parameter that has been widely used to represent as a unique scalar the spectral irradiance function [71, 72]. In our case, and due to the limitations of our spectroradiometer, λ_a and λ_b have been set to 350 and 1100 nm respectively.

Ideally, for estimating the degradation rates, the operating conditions of the module should be the most stable and referred to the same values throughout the period. In addition, to compare the obtained rates with previous works, those measurements should be related to STC: $G_{STC} = 1\,000$ W/m^2 and $T_{STC} = 25$ °C. Unfortunately, the climate of the installation site in Málaga makes such a combination of G and T practically impossible. By choosing the experimental measurements referring to G_{STC} implies to neglect most of the measurements taken in winter period. Therefore, it has been decided to select, within the huge number of experimental measurements available, those ones referring to an irradiance level close to $G_{NOCT} = 800$ W/m^2, thus ensuring that data referring all the seasons of the year are used. After having creamed off the data according to this filter, the center of the temperature range has been fixed individually for each different PV module, by taking the mean temperature value T_c among all the samples within the irradiance range. Regarding the radius of the intervals of G and T, 30 W/m^2 and 1.5 °C respectively have been considered, which are exactly the expanded uncertainty that are estimated for the readings of the pyranometer (Kipp & Zonen CM–21) and the cell temperature sensor (RTD Pt100 class A).

2.4. Degradation model

In some previous studies, the degradation along the time is considered as linear at a first approximation, so that a Simple Linear Regression (SLR) could be used [73]. However, PV modules show different seasonal patterns, especially thin–film devices. This behavior has been known since the 1990s, specially for a–Si:H, as it is stated by Rüther and Livingstone [74], and other previous works [75–77]. These are due to variations in the solar spectrum along the year and, for amorphous silicon modules, to thermal annealing, which can partially recover the initial losses due to light induced degradation [78].

The history profile of a PV thin–film module and its impact depend on the location. However, there are some attempts in the literature that are aimed at separating the seasonality due to the thermal and radiative history of the module from those related to the variability of the actual incident spectrum. Pierro et al. [79] propose a model to estimate the individual contribution on the output performance of each influential variable.

In order to distinguish between the seasonal annual trend and the long–term underlying degradation of thin–film devices, the sequence of values of each electrical parameter should be fitted to a model that allows to separate each component. Some approaches are framed inside the time–series forecasting methods, with very low computational complexity, that have previously been used to study PV degradation, such as Autorregressive Integrated Moving Average (ARIMA) [80] or Seasonal–Trend decomposition by Loess (STL) [81]. These methods require daily or monthly time series, in such a way, after performing the filter by irradiance and temperature, it is necessary to integrate the instantaneous measurements to obtain a discrete equispaced sequence of values, introducing additional uncertainty.

Another approach that can deal with non–equispaced data and with missing information (e.g., several days without measurements) was proposed by [82], consisting on a non–linear model which include several additive terms, including a sinusoidal one to catch the seasonal trend. A fitting routine for non–linear models is available within any mathematical software, e.g., *lsqcurvefit* in Matlab R2021b [83], that implements the trust–region–reflective algorithm to set a value for each free parameter of the model within a feasible interval. Despite its high computational requirements, with the computing power of today's microprocessors, this task requires only a few seconds of execution.

In the same line of that previous work, *we propose the following new model*, in which the variation of each indicator $F(t)$ can be modeled through (eq. 2), assuming that t is expressed in *years* and t_0 is the date of the first measurement:

$$F(t) = \underbrace{(K_0 + K_1 \cdot (t - t_0))}_{\text{long–term}} \cdot (1 + \underbrace{K_2 \cdot \sin(2\pi \cdot (t - t_0 + K_3))}_{\text{seasonal–term}}) \tag{2}$$

where the first term represents a linear long–term degradation, and the second term contains the information on the seasonal variations, which are mostly due to spectral effects or annealing.

There are some important differences between the proposed model and the one used by [82]. On the one hand, the model proposed in that work assumes a logarithmic long–term component in order to deal with the initial strong degradation. However, as the first 8 weeks of exposure are not included in the present study, the model presented in [82] has been simplified by approximating the long–term component by a linear trend. On the other hand, it has physical sense that the amplitude of the seasonal trend, which is the factor multiplying the sinusoidal term, is a percentage of

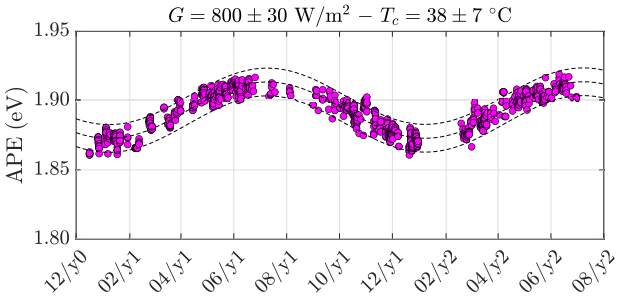

Figure 1: Evolution of the APE during the exposure period, restricted to $G = 800 \pm 30$ W/m^2 – $T_c = 38 \pm 7$ °C.

	K_0	K_1	K_2	K_3
APE	1.893 eV	–	−1.07e-2	+0.175 years

Table 3
Fitting parameters K_i for data of APE.

a base value determined by the long–term component. Therefore, instead of using an additive model of the long–term and the seasonal–term, in (eq. 2) it is proposed a base value that could change over time, $K_0 + K_1 \cdot (t - t_0)$, and let the seasonal part vary as a ratio K_2 of that base value. In this way, assuming that t is expressed in years, the slope K_1 represents the absolute variation of the parameter for each year (e.g., in case of $P_{\max}$, its unit is W/year), whereas K_0 is equal to the value of such parameter at the initial time t_0. Therefore, a relative annual degradation rate can be estimated as a ratio between K_1 and K_0, i.e., DR(%/year) $= 100 \cdot (K_1/K_0)$. Finally, the parameter K_3, which is expressed in years, represents a phase value that allows a delay between the behavior of the different electrical parameters.

3. Results and discussion

First, the evolution of APE value is shown in Figure 1 restricted to the ranges $G = 800 \pm 30$ W/m^2 and $T_c = 38 \pm 7$ °C, that covers the irradiance and temperature ranges assumed for all PV modules under study. During the summer months the APE is higher, which indicates a solar spectrum shifted to the blue, whereas in the winter the APE is lower, indicating a shift towards the red. To have a reference of the evolution of the APE, these data have been fitted to the model in Section 2.4. However, as the solar spectrum is not assumed to be affected by any long–term variation, in this case we propose to fit only the seasonal part of the model, in other words, before performing the fitting procedure we will set the value $K_1(\text{APE}) = 0$. The parameters K_i in Table 3 describe the behavior of the APE during the exposure period. The value $K_0(\text{APE}) = 1.893$ is an estimation of the APE (in eV) on $t = t_0$, i.e., on the first registered day. The value $K_2(\text{APE}) = -1.07\text{e-}2$ is the amplitude of the seasonal variation of the APE. Finally, $K_3(\text{APE}) = 0.175$ (expressed in years) is the delay of the initial day t_0 with respect the natural beginning of the APE sinusoidal oscillation (around 64 days).

For comparative purposes, in this paper the APE evolution (calculated on the complete wavelength range provided by the spectrometer) is provided to explain the annual seasonal trend of the main electrical parameters. It could be possible to cancel the seasonal spectral influence by using a correction based on APE data, but in that case it would be necessary to apply different wavelength limits depending on each technology under test. However, in this work the APE data have not been used to perform any correction to the measurements to avoid additional uncertainties on the degradation rates.

The evolution of the main electrical parameters and the parasitic resistances for each of the four modules, extracted from the experimental measurements, is shown in Figures 2–5. The dotted lines show the interval in which the majority (indicate a quantitative portion) of the points are contained and they are represented to guide the eye.

Before fitting the degradation model of Section 2.4, a first irradiance filter has been applied to the dataset of measurements of all PV modules ($G = 800 \pm 30$ W/m^2). However, a second filter based on the cell temperature

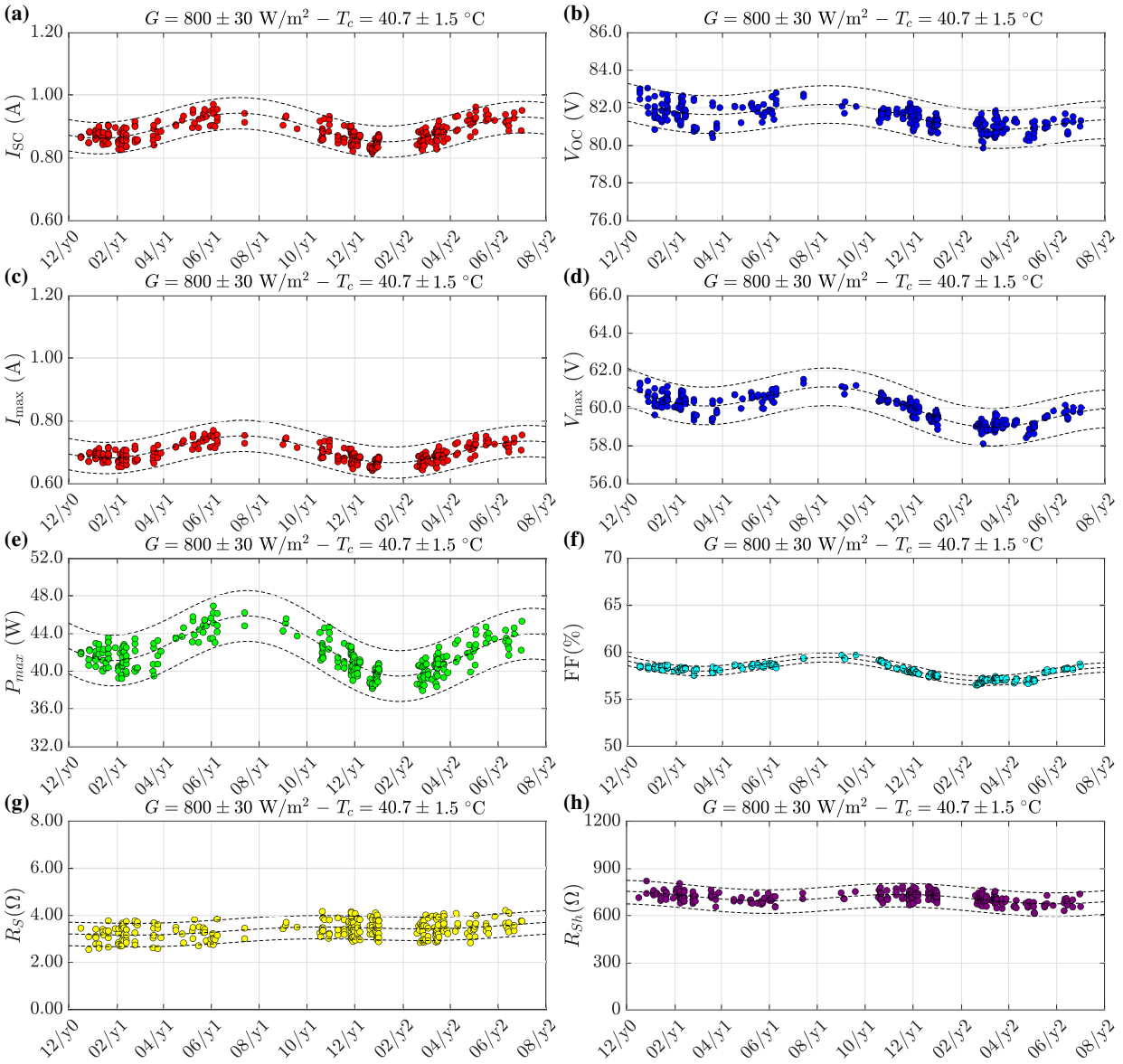

Figure 2: Evolution of main electrical parameters and parasitic resistances for module M1 (a–Si:H)

has also been applied to each PV module. In order to ensure a high number of selected points to fit the model, for every PV module, a different center of the temperature interval has been set, assuming the mean temperature value T_c among all the samples within the previous irradiance range (with a fixed radius of 1.5 °C for all the cases). The results shown in Figure 1 and in Figures 2–5 and indicate a strong correlation of the modules electrical parameters and parasitic resistances with the month of the year and, consequently, with the APE. As it has been stated in Section 1, this seasonal variation makes impossible to compare two measurements taken on different days of the year to quantify the degradation. In general, the electrical parameters experiment a long–term degradation that is superposed to the seasonal trend. The experimental results of the main electrical parameters have also been fitted to the degradation model described in Section 2.4. Tables 4–7 show, in addition to the K_i parameters estimated in each fitting, the value of the degradation rate calculated for each electrical parameter and each module type.

	K_0	K_1	K_2	K_3	DR
I_{SC}	0.907 A	−0.012 A/year	−4.75e-2	+0.190 years	**−1.3%/year**
V_{OC}	82.31 V	−0.81 V/year	−5.51e-3	+0.046 years	**−1.0%/year**
I_{max}	0.723 A	−0.016 A/year	−5.45e-2	+0.171 years	**−2.2%/year**
V_{max}	61.19 V	−1.15 V/year	−1.27e-2	+0.055 years	**−1.9%/year**
P_{max}	44.22 W	−1.77 W/year	−6.42e-2	+0.151 years	**−4.0%/year**
FF	59.23 %	−1.05 %/year	−1.67e-2	+0.066 years	**−1.8%/year**
R_S	3.177 Ω	+0.272 Ω/year	−2.79e-2	−0.013 years	**+8.6%/year**
R_{Sh}	728.6 Ω	−19.7 Ω/year	−3.55e-2	−0.181 years	**−2.7%/year**

Table 4
Parameters K_i and degradation rates of M1

3.1. Amorphous-Si module

For the module M1, of a-Si:H technology, all the electrical parameters (I_{SC}, I_{max}, V_{OC}, V_{max}, P_{max}) show seasonal variations which are directly correlated to the APE variation, i.e. they increase in the summer months and decrease in winter. The value $K_2(P_{max})$ (see Table 4) gives as a measurement of the amplitude of this seasonal variation, leading to a 6.4%, which have been attributed to different effects such as temperature annealing [84] and spectral effects [85]. Rüther et al. [86] suggest that one of the reasons for this behavior could also be a field driven transport in the amorphous material. This seasonal change is so strong that mask the long–term degradation, but the model is able to separate them.

We must highlight the fact that the value of $K_3(I_{SC})$ and the same parameter obtained when fitting the APE values are very close. This means that the current output of this type of modules has a little phase–shift with respect the variations of the solar spectral distribution. The decrease of the short–circuit current of a–Si modules when the spectrum shifts towards longer wavelengths (red) has been reported before in other studies [84] and it is a direct consequence of the lower spectral response of these modules in the longer wavelength range, which is caused by their large direct band gap.

In our case, the annual degradation rate is 4.0%, that is within the upper range stated by other works in the literature referred to this technology. First, some studies have analyzed the dependence of the degradation rate on the electrical load, showing that degradation for a–Si modules can be larger in open–circuit conditions [87], as it is our case. In the review work conducted by Jordan and Kurtz [88], the reported degradation rates for a–Si PV modules were highly dispersed and going up to 4.5%. Returning to Table 1, it is possible to see lower estimations [6, 12, 18–20], but also higher ones [4, 17, 25].

Silvestre et al. [14] study a specimen of the same manufacturer and model, obtaining a lower annual degradation rate (around 2.3%). This module M1 has obtained the worst power degradation rate of all the modules under study, due to a combination of a high decrement of I_{SC} (1.3%/year, more than any other module), a decrement of V_{OC} (1.0%, again more than any other module), and an increase of the R_S (8.6%/year). From Figure 2g, it can be seen that R_S maintains stable during the cool months, whereas the increments happen during the hottest months of the year. This effect due to temperature is inverse to the effect of the annealing, so the beneficial effects of temperature are counteracted in this way. On the other hand, the R_{Sh} has not experienced a significant variation (only a decrement of 2.7%, that is very low assuming the high uncertainty associated to the estimation of this parameter).

	K_0	K_1	K_2	K_3	DR
I_{SC}	2.601 A	−0.025 A/year	−2.53e-2	+0.226 years	**−1.0%/year**
V_{OC}	54.57 V	−0.18 V/year	−1.40e-3	−0.147 years	**−0.3%/year**
I_{max}	2.100 A	−0.045 A/year	−2.99e-2	+0.190 years	**−2.1%/year**
V_{max}	41.52 V	−0.56 V/year	−4.87e-3	−0.032 years	**−1.3%/year**
P_{max}	87.20 W	−3.00 W/year	−3.10e-2	+0.166 years	**−3.4%/year**
FF	61.43 %	−1.33 %/year	−1.14e-2	+0.043 years	**−2.2%/year**
R_S	0.722 Ω	0.165 Ω/year	−3.30e-2	−0.166 years	**+23%/year**
R_{Sh}	163.4 Ω	−12.2 Ω/year	−3.54e-2	+0.017 years	**−7.5%/year**

Table 5
Parameters K_i and degradation rates for module M2

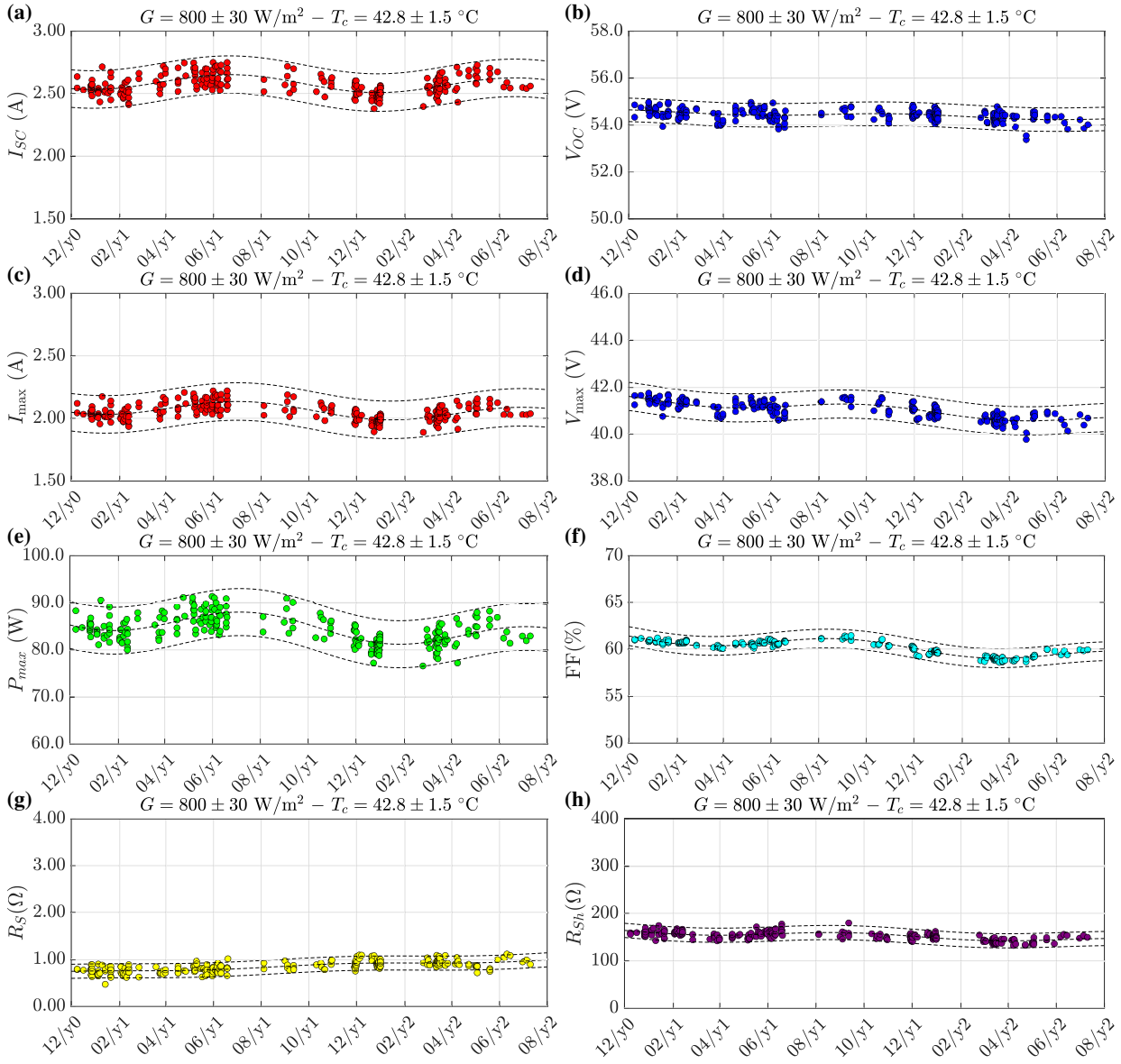

Figure 3: Evolution of main electrical parameters and parasitic resistances for module M2 (a–Si/μc–Si)

3.2. Tandem Amorphous–Si and Microcrystalline–Si module

In case of the module M2 (a–Si/μc–Si), again the studied electrical parameters are affected by a strong seasonal trend, as it can be seen in Figure 3 and Table 5. However, whereas the maximum values of I_{SC} and I_{max} are in summer and the minimum ones in winter, the behavior V_{OC} and V_{max} leads to the highest values in the autumn and the lowest values in spring. The magnitude of the seasonal oscillations in terms of maximum power is quantified by $K_2(P_{max})$ (3.1%). Part of it is due to the spectral variation, and the rest should be due to annealing. As it can be seen, the influence of the annealing is less than in case of a–Si:H, as it is stated by Silvestre et al. [14]. The annual degradation in terms of I_{SC} is almost as high as in case of a–Si (1.0%/year), but the degradation rate of V_{OC} is significant lower (only 0.3%). However, the most serious problem of this PV module was the very high increment of the series resistance R_S (23%/year), much more than any other module under study. On the other hand, R_{Sh} has experienced a moderate decrement (7.5%/year). In balance, the power annual degradation rate of this M2 specimen is 3.4%, significantly higher than the results stated by [8–11], but in the same range than the work by [15]. However, some surveys [29, 30] report even negative degradation rates, although it could be due to under–rating, light–soaking or spectral mismatch issues.

3.3. CdTe/CdS module

Figure 4 shows the tendency observed for the electrical parameters of the module M3, based on CdTe. As opposed to what happens in a–Si modules, in this case only the currents I_{SC}, I_{max} are directly correlated with APE, whereas the voltages V_{OC}, V_{max} show the opposite tendency, having maximum values when APE is lowest. The amplitude of this seasonal trend in terms of power is given by the value $K_2(P_{max})$=1.90%, much lower than for the other studied technologies. This opposite tendency of I_{SC} and V_{OC} in CdTe modules has also been observed in previous literature [89]. Instead of reporting the evolution of the values of P_{max}, in that paper those data are expressed in terms of instant efficiency (the same information normalizing by the module area).

The obtained annual degradation rates for the module M3 is shown in Table 6. For the maximum power, we obtained an annual degradation rate of 3.5%/year for the CdS/CdTe module. As I_{SC} has experience a very low degradation rate (only 0.4%/year) and V_{OC} does not have a strong decrement (0.7%/year), the main contribution to the power drop is related to the evolution of both parasitic resistances: an important increment of the R_S (13%/year), and especially, a very high degradation of the R_{Sh} (26%/year). This abnormal increment of the shunt resistance could be due to the fact that this module is not provided with a frame, in such a way it is more prone to have problems related to humidity that significantly influences this parameter. As it happens with module M1 and M2, the increments of R_S take place in the summer and early autumn, whereas in the rest of the year the value is very stable.

Although there are suspicious papers [21, 26, 90] giving power drops around 0.6%/year (some authors have a contractual relationship with the manufacturer), many works report annual degradation rates for P_{max} from 2 to 6% [4, 7, 14, 18, 19], that is in agreement to our result.

3.4. CIGS module

Some previous considerations should be taken into account. This cylindrical module has a construction not comparable to the one of the conventional PV modules having very different mechanical, electrical, thermal and optical

	K_0	K_1	K_2	K_3	**DR**
I_{SC}	0.962 A	−0.004 A/year	−2.26e-2	+0.242 years	**−0.4%/year**
V_{OC}	82.64 V	−0.56 V/year	+5.62e-3	+0.063 years	**−0.7%/year**
I_{max}	0.827 A	−0.015 A/year	−2.00e-2	−0.218 years	**−1.8%/year**
V_{max}	61.17 V	−1.07 V/year	+8.37e-3	+0.084 years	**−1.7%/year**
P_{max}	50.60 W	−1.75 W/year	+1.90e-2	−0.149 years	**−3.5%/year**
FF	63.68 %	−1.55 %/year	+8.86e-3	+0.096 years	**−2.4%/year**
R_s	7.663 Ω	1.031 Ω/year	+2.32e-2	−0.248 years	**+13%/year**
R_{Sh}	1766.0 Ω	−457.1 Ω/year	+1.31e-1	+0.078 years	**−26%/year**

Table 6
Parameters K_i and degradation rates of module M3

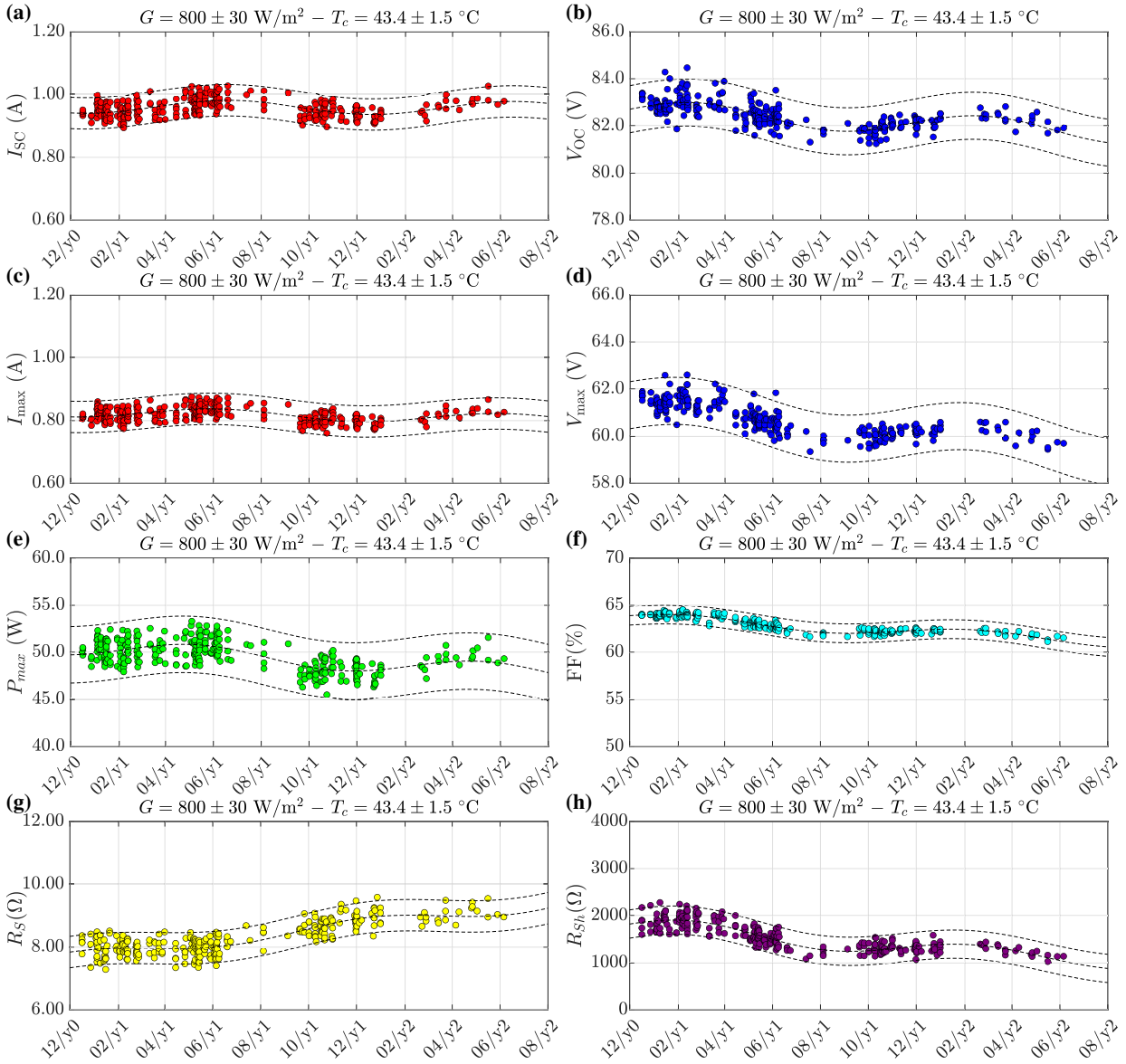

Figure 4: Evolution of main electrical parameters and parasitic resistances for module M3 (CdS/CdTe)

properties [91]. On the one hand, the irradiance received by this module cannot be estimated from the reading provided by the pyranometer installed on the same plane, because this module receives light in a different way that the other planar modules and it is thought to be installed horizontally on the floor, not on an open–rack structure. On the other hand, due to its special shape, the RTD sensors could not be installed in the same way that in the other specimens, and for that reason the value of cell temperature acquired by the measurement system could not be comparable to the readings of the other modules under study (in fact, for this M4 module the registered temperature is abnormally lower than the ones associated to M1, M2 and M3 under the same conditions). All these elements can explain the discrepancy between the measured values in our facilities and the specifications in Table 2. Even so, since these conditions have been maintained throughout the entire exposure period, it is possible to determine a relative degradation rate.

Figure 5 shows the tendency observed for the electrical parameters of module M4 (CIGS). Like in the case of CdTe, I_{SC} and I_{max} are directly correlated with APE, whereas V_{OC} and V_{max} show the opposite tendency, having maximum values when APE is lowest. CI(G)S PV modules normally have a lower dependence on spectrum variations

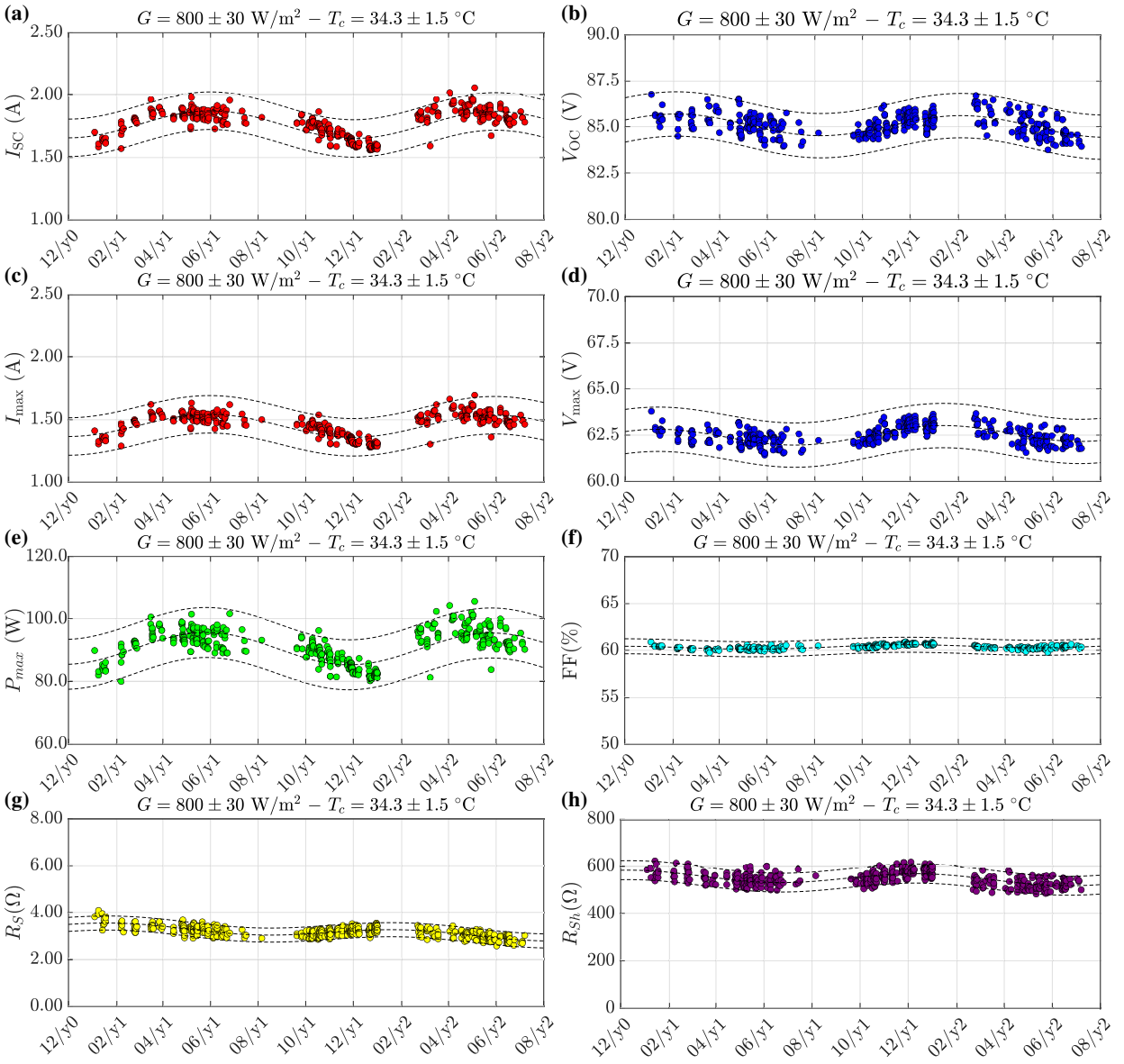

Figure 5: Evolution of main electrical parameters and parasitic resistances for module M4 (CIGS)

compared to other thin–film modules, as their spectral response has a much wider bandwidth. For example, in [84] there was almost no variation detected in the short–circuit current of these modules when plotted against the AM value. However, from Table 7, the magnitude of $K_2(P_{\text{max}}) = 6.67\%$ indicates a strong seasonal variability that cannot be explained by the APE variation. Therefore, there must be other effects affecting the behavior of the CIGS module.

	K_0	K_1	K_2	K_3	DR
I_{SC}	1.766 A	−0.005 A/year	+6.21e-2	−0.208 years	**−0.3%/years**
V_{OC}	85.16 V	−0.09 V/year	+6.63e-3	+0.108 years	**−0.1%/years**
I_{max}	1.454 A	−0.007 A/year	+6.22e-3	−0.207 years	**−0.5%/years**
V_{max}	62.33 V	+0.20 V/year	−7.65e-3	−0.315 years	**+0.3%/years**
P_{max}	90.60 W	−0.150 W/year	+5.67e-2	−0.193 years	**−0.2%/years**
FF	60.23 %	+0.16 %/year	−3.27e-3	−0.178 years	**+0.3%/years**
R_S	3.401 Ω	−0.270 Ω/year	+5.63e-2	+0.1186 years	**−7.9%/years**
R_{Sh}	561.3 Ω	−14.0 Ω/year	−4.05e-2	−0.252 years	**−2.5%/years**

Table 7
Parameters K_i and degradation rates of module M4

On the one hand, the series resistance of the CIGS module is decreasing in time. There are very few previous studies that analyze the evolution of series and parallel resistances as a CIGS module degrades. For example, Del Cueto et al. [31] compare the trend of a couple of CIGS modules from two manufacturers exposed outdoor throughout 5.5 years, obtaining different results: whereas one of them experiment an increment from 1.3 to 1.7 Ω (5.6% each year), the other one remains around 1.3 Ω all the period. On the other hand, the behavior of R_{Sh} reflects an almost insignificant decrement of this parameter (2.5%), taking into account that this is the one with highest uncertainty.

Degradation mechanisms in CIGS cells have been associated to shunting due to the formation of leakage paths across the p-n junction resulting from defect states associated to lattice mismatch at the hetero–junction [84]. The manufacturer claims that, based on its own accelerated and on–field tests, the annual power degradation rate is less than 0.5% [92]. This could be in line with the results presented in this paper, because the estimated degradation is not significant (an annual degradation in power around 0.2%/year). The degradation rates in term of current and voltage are also very low (0.3%/year and 0.1%/year respectively). This also agrees with the results discussed in Musikowski and Styczynsk [93], which reports any degradation after 6 years of operation connected to a solar inverter. However, there are survey reports that state much higher averaged annual degradation rates for CIGS modules, such as 1.17% or 1.28% [29, 30].

4. Conclusions

A degradation analysis has been performed from outdoor measurements of four thin–film photovoltaic modules that have been exposed for 20 months. Each specimen has been characterized at regular intervals of time in such a way it has been possible to perform a selection of samples within a very narrow range of irradiance and cell temperature to plot the evolution of the electrical parameters and of the parasitic resistances. The results show a strong seasonal variation due to changes in the APE of the sun spectral distribution and other phenomena as annealing. To distinguish this annual variation from the long–term degradation, each filtered set of samples has been fitted to a novel degradation model, which allows to estimate the annual degradation rates of the different indicators for each specimen.

Regarding the a-Si:H technology, both I_{SC} and V_{OC} are synchronized to the variation of the APE estimated from the spectrum. In this case, the highest annual degradation rate in terms of power has been estimated (4.0%/year), among all the PV modules analyzed in this paper, that could be due to a combination of the strongest decrease of I_{SC} (1.3%/year) and V_{OC} (1.0%/year), in addition to a significant increase of R_S (8.6%/year). Although there is a great dispersion of the degradation rates reported previously, the results presented in the paper are within the upper range stated in the literature referred to a-Si:H.

With respect the a–Si/μc–Si specimen, again the main electrical parameters follow the tendency of the APE evolution, but in the case of V_{OC} and P_{max} with more delay than in the case of a-Si:H. The annual degradation rate in terms of power is also significantly high (3.4%/year), especially if it is compared to the one documented in other published studies. Having high annual degradation for I_{SC} (1.0%/year), the degradation rate in terms of V_{OC} is significantly lower (0.3%/year). However, R_S has suffered the highest increment of all the modules (23%/year), in addition to a significant but lower degradation of R_{Sh} (7.5%/year).

For the module based on CdTe/CdS technology, contrary to modules based on amorphous silicon, the evolution of V_{OC} and V_{max} is opposite to I_{SC} and I_{max}; thus, the voltage values are the highest when APE is the lowest, but with a reduced amplitude of the seasonal trend in comparison to the other specimens. The obtained annual degradation rate is also very significant (3.4%/year) for the CdS/CdTe module, due mainly to very high degradation of both parasitic resistances, an increment of R_S around 13%/year, and a strong decrease of R_{Sh} reaching 26%/year.

Finally, as for the Solyndra module (CIGS), despite of all the difficulties related to the very different features of this special device, an estimation of its annual degradation rate in terms of power has been determined. Again, its V_{OC} behavior is reversed with respect the one observed for I_{SC}. The most impacting fact about this specimen is the decrease of R_S throughout time that, in addition to a very low degradation of V_{OC} and I_{SC}, leads us to an insignificant annual degradation rate (0.2%/year); that is in agreement with the results presented by some other authors.

Some final considerations should be made at the end. First, the length of the exposure stabilization period is not a point clearly established in previous literature, and it is an open point of discussion. In any case, this issue could be an important source of discrepancy of the results obtained by different authors. Another controversial element is the total length of the exposure period; thus, a longer one could lead to more representative long–term degradation rates. Finally, the post–processing of the measured data and the model used to remove the seasonal trend could have an important impact on the final results; thus, it is necessary to avoid data manipulation or correction procedures as far as possible, as it has been done in this paper.

The study presented in this article is focused on the degradation of thin–film technologies at module level. It would be desirable to extend the scope in order to analyse the power drop associated to complete PV generators. Unfortunately, the scarcity of installations based on these technologies and the difficulty to have the required permissions and access to the necessary data remain challenges to be overcome.

Funding:

Ministero dell'Istruzione, dell'Università e della Ricerca (Italy) [grant PRIN2020–HOTSPHOT 2020LB9TBC and grant PRIN2017–HEROGRIDS 2017WA5ZT3_003]; *Università degli Studi di Salerno* [FARB funds]; *Ministerio de Ciencia, Innovación y Universidades (Spain)* [grant RTI2018-095097–B–I0].

CRediT authorship contribution statement

Michel Piliougine: Conceptualization, Methodology, Software, Validation, Data Curation, Writing – Original Draft, Writing – Reviewing and Editing, Visualization. **Paula Sánchez-Friera:** Methodology, Validation, Writing – Original Draft, Writing – Reviewing and Editing. **Giovanni Petrone:** Methodology, Writing – Original Draft, Writing – Reviewing and Editing. **Francisco José Sánchez-Pacheco:** Methodology, Writing – Original Draft, Writing – Reviewing and Editing. **Giovanni Spagnuolo:** Methodology, Writing – Original Draft, Writing – Reviewing and Editing. **Mariano Sidrach-de-Cardona:** Methodology, Writing – Original Draft, Writing – Reviewing and Editing.

References

[1] A. Jaeger-Waldau, PV Status Report 2010, EUR 24344, Office for Official Publications of the European Union, Luxembourg, 2010. URL: https://doi.org/10.2788/87966.

[2] L. V. Mercaldo, M. L. Addonizio, M. D. Noce, P. D. Veneri, A. Scognamiglio, C. Privato, Thin film silicon photovoltaics: Architectural perspectives and technological issues, Appl Energ 86 (2009) 1836–1844. URL: https://doi.org/10.1016/j.apenergy.2008.11.034.

[3] E. H. Rusnindyo, E. A. Karuniawan, A. A. Setiawan, F. D. Wijaya, Building integrated thin film photovoltaic performance modelling on conventional building, AIP Conf Proc 2255 (2020) 070023. URL: https://doi.org/10.1063/5.0014597.

[4] D. A. Cassini, S. C. S. Costa, A. S. A. Diniz, L. L. Kazmerski, Evaluation of failure modes for photovoltaic modules in arid climatic zones in Brazil, in: 48th IEEE Photovoltaic Specialists Conference (PVSC), 2021, pp. 0580–0582. URL: https://doi.org/10.1109/PVSC43889.2021.9518798.

[5] M. Kumar, A. Kumar, R. Gupta, Comparative degradation analysis of different photovoltaic technologies on experimentally simulated water bodies and estimation of evaporation loss reduction, Prog Photovoltaics 29 (2021) 357–378. URL: https://doi.org/10.1002/pip.3370.

[6] R. Singh, M. Sharma, R. Rawat, C. Banerjee, Field analysis of three different silicon-based technologies in composite climate condition – Part II – Seasonal assessment and performance degradation rates using statistical tools, Renew Energ 147 (2020) 2102–2117. URL: https://doi.org/10.1016/j.renene.2019.10.015.

[7] S. Kichou, P. Wolf, S. Silvestre, A. Chouder, Analysis of the behaviour of cadmium telluride and crystalline silicon photovoltaic modules deployed outdoor under humid continental climate conditions, Sol Energy 171 (2018) 681–691. URL: https://doi.org/10.1016/j.solener.2018.07.028.

[8] N. Aarich, M. Raoufi, A. Bennouna, N. Erraissi, Outdoor comparison of rooftop grid–connected photovoltaic technologies in Marrakech (Morocco), Energ Buildings 173 (2018) 138–149. URL: https://doi.org/10.1016/j.enbuild.2018.05.030.

[9] A. Limmanee, S. Songtrai, N. Udomdachanut, S. Kaewniyompanit, Y. Sato, M. Nakaishi, S. Kittisontirak, K. Sriprapha, Y. Sakamoto, Degradation analysis of photovoltaic modules under tropical climatic conditions and its impacts on LCOE, Renew Energ 102 (2017) 199–204. URL: https://doi.org/10.1016/j.renene.2016.10.052.

[10] T. Ozden, B. G. Akinoglu, R. Turan, Long term outdoor performances of three different on–grid PV arrays in central Anatolia – An extended analysis, Renew Energ 101 (2017) 182–195. URL: https://doi.org/10.1016/j.renene.2016.08.045.

[11] A. Tahri, S. Silvestre, F. Tahri, S. Benlebna, A. Chouder, Analysis of thin film photovoltaic modules under outdoor long term exposure in semi-arid climate conditions, Sol Energy 157 (2017) 587–595. URL: https://doi.org/10.1016/j.solener.2017.08.048.

[12] S. Kichou, S. Silvestre, G. Nofuentes, M. Torres-Ramírez, A. Chouder, D. Guasch, Characterization of degradation and evaluation of model parameters of amorphous silicon photovoltaic modules under outdoor long term exposure, Energy 96 (2016) 231–241. URL: https://doi.org/10.1016/j.energy.2015.12.054.

[13] S. Kichou, E. Abaslioglu, S. Silvestre, G. Nofuentes, M. Torres-Ramírez, A. Chouder, Study of degradation and evaluation of model parameters of micromorph silicon photovoltaic modules under outdoor long term exposure in Jaén, Spain, Energ Convers Manage 120 (2016) 109–119. URL: https://doi.org/10.1016/j.enconman.2016.04.093.

[14] S. Silvestre, S. Kichou, L. Guglielminotti, G. Nofuentes, M. Alonso-Abella, Degradation analysis of thin film photovoltaic modules under outdoor long term exposure in Spanish continental climate conditions, Sol Energy 139 (2016) 599–607. URL: https://doi.org/10.1016/j.solener.2016.10.030.

[15] P. Ferrada, F. Araya, A. Marzo, E. Fuentealba, Performance analysis of photovoltaic systems of two different technologies in a coastal desert climate zone of Chile, Sol Energy 114 (2015) 356–363. URL: https://doi.org/10.1016/j.solener.2015.02.009.

[16] A. Kyprianou, A. Phinikarides, G. Makrides, G. E. Georghiou, Definition and computation of the degradation rates of photovoltaic systems of different technologies with robust principal component analysis, IEEE J Photovolt 5 (2015) 1698–1705. URL: https://doi.org/10.1109/JPHOTOV.2015.2478065.

[17] V. Sharma, O. Sastry, A. Kumar, B. Bora, S. Chandel, Degradation analysis of a–Si, (HIT) hetro–junction intrinsic thin layer silicon and m–C–Si solar photovoltaic technologies under outdoor conditions, Energy 72 (2014) 536–546. URL: https://doi.org/10.1016/j.energy.2014.05.078.

[18] J. Y. Ye, T. Reindl, A. G. Aberle, T. M. Walsh, Performance degradation of various PV module technologies in tropical Singapore, IEEE J Photovolt 4 (2014) 1288–1294. URL: https://doi.org/10.1109/JPHOTOV.2014.2338051.

[19] G. Makrides, B. Zinsser, M. Schubert, G. E. Georghiou, Performance loss rate of twelve photovoltaic technologies under field conditions using statistical techniques, Sol Energy 103 (2014) 28–42. URL: https://doi.org/10.1016/j.solener.2014.02.011.

[20] R. Gottschalg, T. Betts, A. Eeles, S. Williams, J. Zhu, Influences on the energy delivery of thin film photovoltaic modules, Sol Energ Mat Sol C 119 (2013) 169–180. URL: https://doi.org/10.1016/j.solmat.2013.06.011.

[21] N. Strevel, L. Trippel, M. Gloeckler, Performance characterization and superior energy yield of First Solar PV power plants in high-temperature conditions, Photovoltaics International 17 (2012). URL: https://www.pv-tech.org/technical-papers/performance-characterization-and-superior-energy-yield-of-first-solar-pv-power-plants-in-hightemperature-conditions/.

[22] D. C. Jordan, S. R. Kurtz, Thin-film reliability trends toward improved stability, in: 37th IEEE Photovoltaic Specialists Conference (PVSC), Seattle, WA, USA, 2011, pp. 000827–000832. URL: https://doi.org/10.1109/PVSC.2011.6186081.

[23] J. Del Cueto, S. Rummel, B. Kroposki, C. Osterwald, A. Anderberg, Stability of CIS/CIGS modules at the outdoor test facility over two decades, in: 33rd IEEE Photovoltaic Specialists Conference (PVSC), San Diego, CA, USA, 2008, pp. 1–6. URL: https://doi.org/10.1109/PVSC.2008.4922772.

[24] W. Durisch, K.-H. Lam, J. Close, Efficiency and degradation of a copper indium diselenide photovoltaic module and yearly output at a sunny site in Jordan, Appl Energ 83 (2006) 1339–1350. URL: https://doi.org/10.1016/j.apenergy.2006.02.002.

[25] J. Adelstein, W. Sekulic, Small PV systems performanceevaluation at NREL's outdoortest facility using the PVUSA power rating method, in: 2005 DOE Solar Energy TechnologiesProgram Review Meeting, NREL/CP-520-39135, Denver, CO, USA, 2005. URL: https://www.osti.gov/biblio/882794-small-pv-systems-performance-evaluation-nrel-outdoor-test-facility-using-pvusa-power-rating-method.

[26] B. Marion, J. del Cueto, P. McNutt, D. Rose, Performance summary for the First Solar CdTe 1–kW system, in: 2001 NCPV Program Review Meeting, NREL/CP-520-30942, National Renewable Energy Laboratory NREL, Golden, CO, USA, 2001. URL: https://www.osti.gov/biblio/15000007.

[27] D. C. Jordan, T. J. Silverman, J. H. Wohlgemuth, S. R. Kurtz, K. T. VanSant, Photovoltaic failure and degradation modes, Prog Photovoltaics 25 (2017) 318–326. URL: https://doi.org/10.1002/pip.2866.

[28] D. C. Jordan, S. R. Kurtz, K. VanSant, J. Newmiller, Compendium of photovoltaic degradation rates, Prog Photovoltaics 24 (2016) 978–989. URL: https://doi.org/10.1002/pip.2744.

[29] S. Chattopadhyay, R. Dubey, V. Kuthanazhi, S. Zachariah, S. Bhaduri, C. Mahapatra, All-India Survey of Module Reliability: 2016. National Institute of Solar Energy (India), 2017. URL: https://nise.res.in/wp-content/uploads/2018/01/All-India-Survey-of-Photovoltaic-Module-Reliability-2016-_-Rev2_25012018_online_lowres.pdf.

[30] Y. Golive, S. Zachariah, S. Bhaduri, R. Dubey, S. Chattopadhyay, P. Joshi, All-India Survey of Module Reliability: 2018. National Institute of Solar Energy (India), 2019. URL: https://nise.res.in/wp-content/uploads/2020/01/All-India-Survey-of-Photovoltaic-Module-Reliability_2018_Report.pdf.

[31] J. A. Del Cueto, S. Rummel, B. Kroposki, A. Anderberg, Long-term performance data and analysis of CIS/CIGS modules deployed outdoors, in: B. von Roedern, A. E. Delahoy (Eds.), Photovoltaic Cell and Module Technologies II, volume 7045, International Society for Optics and Photonics, SPIE, San Diego, CA, USA, 2008, pp. 7–17. URL: https://doi.org/10.1117/12.796505.

[32] T. Silverman, U. Jahn, G. Friesen, I. E. A. P. P. S. Programme, Characterisation of performance of thin–film photovoltaic technologies: IEA PVPS Task 13, Subtask 3.1 : Final Report IEA–PVPS T13-02:2014, International Energy Agency, Photovoltaic Power Systems Programme, 2014. URL: https://repository.supsi.ch/5776/1/IEA-PVPS_T13-02_2014_Characterization_ThinFilm_Modules.pdf, ISBN: 978-3-906042-17-6.

[33] D. Dirnberger, Uncertainty in PV module measurement – Part II: Verification of rated power and stability problems, IEEE J Photovolt 4 (2014) 991–1007. URL: https://doi.org/10.1109/JPHOTOV.2014.2307158.

[34] D. L. Staebler, C. R. Wronski, Reversible conductivity changes in discharge–produced amorphous Si, Appl Phys Lett 31 (1977) 292–294. URL: https://doi.org/10.1063/1.89674.

[35] T. Yanagisawa, Long–term degradation tests of amorphous silicon solar cells: Correlation between light– and current–induced degradation characteristics, Microelectron Reliab 35 (1995) 183–187. URL: https://doi.org/10.1016/0026-2714(95/90084-4.

[36] Kaneka Thin Film PV Installation Manual. Module type: G-EA060, KANEKA Corporation, 2009. URL: https://www.dropbox.com/s/8n9w6lc077nhcso/KANEKA_MANUAL.pdf, Last accessed: November 15th, 2021.

[37] M. Muñoz–García, O. Marin, M. Alonso–García, F. Chenlo, Characterization of thin film PV modules under standard test conditions: Results of indoor and outdoor measurements and the effects of sunlight exposure, Sol Energy 86 (2012) 3049–3056. URL: https://doi.org/10.1016/j.solener.2012.07.015.

[38] C. Radue, E. Van Dyk, A comparison of degradation in three amorphous silicon PV module technologies, Sol Energ Mat Sol C 94 (2010) 617–622. URL: https://doi.org/10.1016/j.solmat.2009.12.009.

[39] J. A. Del Cueto, C. A. Deline, S. R. Rummel, A. Anderberg, Progress toward a stabilization and preconditioning protocol for polycrystalline thin–film photovoltaic modules, in: 35th IEEE Photovoltaic Specialists Conference (PVSC), Honolulu, HI, USA, 2010, pp. 002423–002428. URL: https://doi.org/10.1109/PVSC.2010.5614223.

[40] K. Astawa, T. Betts, R. Gottschalg, Effect of loading on long term performance of single junction amorphous silicon modules, Sol Energ Mat Sol C 95 (2011) 119–122. URL: https://doi.org/10.1016/j.solmat.2010.04.071.

[41] D. King, J. Kratochvil, W. Boyson, Stabilization and performance characteristics of commercial amorphous–silicon PV modules, in: 28th IEEEE Photovoltaic Specialists Conference (PVSC), Anchorage, AK, USA, 2000, pp. 1446–1449. URL: https://doi.org/10.1109/PVSC.2000.916165.

[42] J. A. Del Cueto, J. Pruett, D. Cunningham, Stabilization of high efficiency CdTe photovoltaic modules in controlled indoor light soaking, in: National Center for Photovoltaics and Solar Program Review Meeting, NREL/CP-520-33543, Denver, CO, USA, 2003. URL: https://www.osti.gov/biblio/15004239-stabilization-high-efficiency-cdte-photovoltaic-modules-controlled-indoor-light-soaking.

[43] C. Deline, J. A. del Cueto, D. S. Albin, S. Rummel, Metastable electrical characteristics of polycrystalline thin-film photovoltaic modules upon exposure and stabilization, J Photonics Energy 2 (2012) 022001. URL: https://doi.org/10.1117/1.JPE.2.022001.

[44] Resumen Mensual de la radiación solar. Diciembre 2011, Agencia Estatal de Meteorología (AEMET). Ministerio de Medio Ambiente y Medio Rural y Marino. Gobierno de España, 2011. URL: https://www.aemet.es/documentos/es/serviciosclimaticos/vigilancia_clima/radiacion_ozono/radiacion_solar/2011/InformeRad_Solar_2011_12.pdf, Last accessed: November 15th, 2021.

[45] B. H. King, J. S. Stein, D. Riley, C. B. Jones, C. D. Robinson, Degradation assessment of fielded CIGS photovoltaic arrays, in: 44th IEEE Photovoltaic Specialist Conference (PVSC), Washington, DC, USA, 2017, pp. 3155–3160. URL: https://doi.org/10.1109/PVSC.2017.8366332.

[46] A. Kaul, S. Pethe, N. G. Dhere, Long-term performance analysis of copper indium gallium selenide thin-film photovoltaic modules, J Photonics Energy 2 (2012) 022005. URL: https://doi.org/10.1117/1.JPE.2.022005.

[47] M. Demirtaş, B. Tamyürek, E. Kurt, Ípek. Çetinbaş, M. K. Öztürk, Effects of aging and environmental factors on performance of CdTe and CIS thin–film photovoltaic modules, J Electron Mater 48 (2019) 6890–6900. URL: https://doi.org/10.1007/s11664-019-07172-z.

[48] M. Kumar, A. Kumar, Experimental validation of performance and degradation study of canal-top photovoltaic system, Appl Energ 243 (2019) 102–118. URL: https://doi.org/10.1016/j.apenergy.2019.03.168.

[49] A. Virtuani, H. M ullejans, E. D. Dunlop, Comparison of indoor and outdoor performance measurements of recent commercially available solar modules, Prog Photovoltaics 19 (2011) 11–20. URL: https://doi.org/10.1002/pip.977.

[50] IEC 60891:2021, Photovoltaic devices – Procedures for temperature and irradiance corrections to measured I–V characteristics, 3 ed., International Electrotechnical Commission IEC, Geneva (Switzerland), 2021. URL: https://webstore.iec.ch/publication/61766, ISBN: 978-2-8322-1036-0.

[51] M. Piliougine, R. Guejia-Burbano, G. Petrone, F. Sánchez-Pacheco, L. Mora-López, M. Sidrach-de-Cardona, Parameters extraction of single diode model for degraded photovoltaic modules, Renew Energ 164 (2021) 674–686. URL: https://doi.org/10.1016/j.renene.2020.09.035.

[52] E. A. Schiff, S. Hegedus, X. Deng, Amorphous Silicon–based solar cells, in: A. Luque, S. Hegedus (Eds.), Handbook of Photovoltaic Science and Engineering, 2 ed., John Wiley and Sons, Chichester, West Sussex, UK, 2011, pp. 487–545. URL: https://doi.org/10.1002/9780470974704.ch12. doi:10.1002/9780470974704.ch12, ISBN: 978-0-470-72169-8.

[53] Kaneka GEA060 Specification Sheet, KANEKA, Corporation. URL: https://www.dropbox.com/s/mrr7xm5qeyi1iaf/Kaneka_GEA060.pdf, Last accessed: November 15th, 2021.

[54] Solarmodule Phoenix Solar – PHX – 120 – LV, Phoenix Solar, AG. URL: https://www.dropbox.com/s/4ohvib18ink1hqa/PhoenixSolar_PHX120LV.pdf, Last accessed: November 15th, 2021.

[55] First Solar FS Series 2 PV Module, PD-5-401-02, First Solar Inc., 2011. URL: https://www.dropbox.com/s/xmmny6vjzifqo60/FirstSolar.pdf, Last accessed: November 15th, 2021.

[56] Solar modules SOLYNDRA-SL-001-150C/157C/165C/173C/182C. Specification Sheet, sly182-eng-01109, Phoenix Solar, Inc. URL: https://www.dropbox.com/s/d3c7n22y90g4red/Solyndra.pdf, Last accessed: November 15th, 2021.

[57] Solyndra Product Training, Solyndra, Inc. URL: https://www.dropbox.com/s/si3ozo9rxk5o1wg/SolyndraManual.pdf, Last accessed: November 15th, 2021.

[58] Precision Pyranometer CM21 – Instruction Manual, 0304 ed., Kipp & Zonen, Delft, Holland, B.V. URL: https://www.dropbox.com/s/hln7wqhoakb2ax6/KIPPZONEN_cm21.pdf, Last accessed: November 15th, 2021.

[59] Compensated Calibrated Cell – Radiation Sensors, Atersa, Grupo Elecnor, Madrid, España, 2004. URL: https://www.dropbox.com/s/khmn20h9em450d9/atersa.pdf, Last accessed: November 15th, 2021.

[60] Adhesive Silicone Patch Pt100 Temperature Sensors, Industrial Temperature Sensors, ITS. URL: https://www.dropbox.com/s/ae41d240hkw72r3/pt100.pdf, Last accessed: November 15th, 2021.

[61] L. Micheli, J. A. Caballero, E. F. Fernández, G. P. Smestad, G. Nofuentes, T. K. Mallick, F. Almonacid, Correlating photovoltaic soiling losses to waveband and single-value transmittance measurements, Energy 180 (2019) 376–386. URL: https://doi.org/10.1016/j.energy.2019.05.097.

[62] IEC 60904–3, Photovoltaic devices – Part 3: Measurement principles for terrestrial photovoltaic (PV) solar devices with reference spectral irradiance data, 4 ed., International Electrotechnical Commission IEC, Geneva, Switzerland, 2019. URL: https://webstore.iec.ch/publication/61084, ISBN: 978-2-8322-6268-9.

[63] Compact FieldPoint cFP-21xx and cFP-BP-x – User Manual, National Instruments, Austin (TX, USA), 2005. URL: https://www.dropbox.com/s/7gxfnw8zll1ksun/cFP_2120.pdf, Last accessed: November 15th, 2021.

[64] M. Piliougine, J. Carretero, L. Mora-López, M. Sidrach-de-Cardona, Experimental system for current–voltage curve measurement of photovoltaic modules under outdoor conditions, Prog Photovoltaics 19 (2011) 591–602. URL: http://dx.doi.org/10.1002/pip.1073.

[65] M. Piliougine, J. Carretero, L. Mora-López, M. Sidrach-de-Cardona, New software tool to characterize photovoltaic modules from commercial equipment, WEENTECH Proceedings in Energy (2018) 211–220. URL: https://doi.org/10.32438/WPE.6218.

[66] M. Piliougine, A. Oukaja, P. Sánchez-Friera, G. Petrone, F. J. Sánchez-Pacheco, G. Spagnuolo, M. Sidrach-de-Cardona, Analysis of the degradation of single-crystalline silicon modules after 21 years of operation, Prog Photovoltaics 29 (2021) 907–919. URL: https://doi.org/10.1002/pip.3409.

[67] ISO/IEC Guide 98-3, Uncertainty of measurement – Part 3: Guide to the expression of uncertainty in measurement (GUM:1995), 1 ed., International Organization for Standardization ISO, Geneva (Switzerland), 2008. URL: https://www.iso.org/standard/50461.html.

[68] K. Emery, Photovoltaic calibrations at the National Renewable Energy Laboratory and uncertainty analysis following the ISO 17025 guidelines, NREL/TP-5J00-66873, National Renewable Energy Laboratory NREL, Golden, CO, USA, 2016. URL: https://www.nrel.gov/docs/fy17osti/66873.pdf.

[69] F. Toledo, J. M. Blanes, Analytical and quasi-explicit four arbitrary point method for extraction of solar cell single-diode model parameters, Renew Energ 92 (2016) 346–356. URL: https://doi.org/10.1016/j.renene.2016.02.012.

[70] M. Piliougine, D. Elizondo, L. Mora-López, M. S. de Cardona, Photovoltaic module simulation by neural networks using solar spectral distribution, Prog Photovoltaics 21 (2013) 1222–1235. URL: https://doi.org/10.1002/pip.2209.

[71] R. Moreno–Sáez, M. Sidrach–de–Cardona, L. Mora–López, Analysis and characterization of photovoltaic modules of three different thin-film technologies in outdoor conditions, Appl Energ 162 (2016) 827–838. URL: https://doi.org/10.1016/j.apenergy.2015.10.156.

[72] G. Nofuentes, C. Gueymard, J. Aguilera, M. Pérez-Godoy, F. Charte, Is the average photon energy a unique characteristic of the spectral distribution of global irradiance?, Sol Energy 149 (2017) 32–43. URL: https://doi.org/10.1016/j.solener.2017.03.086.

[73] S. Lindig, I. Kaaya, K.-A. Weiss, D. Moser, M. Topic, Review of statistical and analytical degradation models for photovoltaic modules and systems as well as related improvements, IEEE J Photovolt 8 (2018) 1773–1786. URL: https://doi.org/10.1109/JPHOTOV.2018.2870532.

[74] R. Rüther, J. Livingstone, Seasonal variations in amorphous silicon solar module outputs and thin film characteristics, Sol Energ Mat Sol C 36 (1995) 29–43. URL: https://doi.org/10.1016/0927-0248(94/00165-0.

[75] P. Ragot, H. Costa, D. Desmettre, Higher efficiency new generation amorphous silicon PV modules, in: 11th European Photovoltaic Solar Energy Conference, Montreux, Switzerland, 1992, pp. 553–555.

[76] G. Kleiss, K. Bücher, A. Raicu, K. Heidler, Performance of thin film solar cells under realistic reporting conditions including degradation effects, in: 11th European Photovoltaic Solar Energy Conference, Montreux, Switzerland, 1992, pp. 578–581.

[77] P. Ragot, J. L. Martin, Performance of thin film solar cells under realistic reporting conditions including degradation effects, in: 13th European Photovoltaic Solar Energy Conference, Nice, France, 1995, pp. 2315–2318.

[78] A. Carr, T. Pryor, A comparison of the performance of different PV module types in temperate climates, Sol Energy 76 (2004) 285–294. URL: https://doi.org/10.1016/j.solener.2003.07.026.

[79] M. Pierro, F. Bucci, C. Cornaro, Impact of light soaking and thermal annealing on amorphous silicon thin film performance, Prog Photovoltaics 23 (2015) 1581–1596. URL: https://doi.org/10.1002/pip.2595.

[80] A. Phinikarides, G. Makrides, N. Kindyni, A. Kyprianou, G. E. Georghiou, ARIMA modeling of the performance of different photovoltaic technologies, in: 39th IEEE Photovoltaic Specialists Conference (PVSC), Tampa, FL, USA, 2013, pp. 0797–0801. URL: https://doi.org/10.1109/PVSC.2013.6744268.

[81] S. A. Tabatabaei, D. Formolo, J. Treur, Analysis of performance degradation of domestic monocrystalline photovoltaic systems for a real–world case, Energ Proc 128 (2017) 121–129. URL: https://doi.org/10.1016/j.egypro.2017.09.025.

[82] I. Muirhead, B. Hawkins, Research into new technology photovoltaic modules at Telstra Research Laboratories – What we have learnt, in: Annual Conference of the Australian and New Zealand Solar Energy Society - SOLAR '96, Darwin, Northern Territory, Australia, 1996. URL: https://www.dropbox.com/s/874wolo29tvfgov/Solar96.PDF.

[83] Matlab Optimization Toolbox. User's guide. R2021b, MathWorks, Natick (MA, USA), 2021. URL: https://www.dropbox.com/s/y9c49mj118hkd8l/optim.pdf.

[84] E. Meyer, E. van Dyk, Characterization of degradation in thin-film photovoltaic module performance parameters, Renew Energ 28 (2003) 1455–1469. URL: https://doi.org/10.1016/S0960-1481(02/00062-9.

[85] J. Merten, J. Andreu, Clear separation of seasonal effects on the performance of amorphous silicon solar modules by outdoor iv measurements, Sol Energ Mat Sol C 52 (1998) 11–25. URL: https://doi.org/10.1016/S0927-0248(97/00263-8.

[86] R. Rüther, G. Kleiss, K. Reiche, Spectral effects on amorphous silicon solar module fill factors, Sol Energy Mater Sol Cells 71 (2002) 375–385. URL: https://doi.org/10.1016/S0927-0248(01/00095-2.

[87] L. Fanni, I. Pola, E. Burà, T. Friesen, D. Chianese, Investigation of annealing and degradation effects on a-Si PV modules in real operating conditions, in: 24th European Photovoltaic Solar Energy Conference (EU PVSEC), Hamburg, Germany, 2009, p. 3596–3599. URL: https://doi.org/10.4229/24thEUPVSEC2009-4AV.3.92.

[88] D. Jordan, S. R. Kurtz, Photovoltaic degradation rates – an analytical review, Prog Photovoltaics 21 (2013) 12–29. URL: https://doi.org/10.1002/pip.1182.

[89] J. A. Del Cueto, Review of the field performance of one cadmium telluride module, Prog Photovoltaics 6 (1998) 433–446. URL: https://doi.org/10.1002/(SICI/1099-159X(199811/12/6:6<433::AID-PIP236>3.0.CO;2-L.

[90] L. Ngan, N. Strevel, K. Passow, A. F. Panchula, D. Jordan, Performance characterization of cadmium telluride modules validated by utility-scale and test systems, in: 40th IEEE Photovoltaic Specialist Conference (PVSC), Denver, CO, USA, 2014, pp. 1957–1962. URL: https://doi.org/10.1109/PVSC.2014.6925309.

[91] H. Hiraki, A. Hiraki, M. Maeda, Y. Takahashi, Unique features of cylindrical type solar–module contrasted with plane or conventional type ones, J Phys Conf Ser 371 (2012) 012002. URL: https://doi.org/10.1088/1742-6596/379/1/012002.

[92] C. M. Gronet, Solyndra, Inc. Amendment No. 1 To Form S-1 Registration Statement, Reg. number 333-163845, 2010. URL: https://www.sec.gov/Archives/edgar/data/0001443115/000119312510058567/ds1a.htm, Last accessed: November 15th, 2021.

[93] H. D. Musikowski, Z. A. Styczynsk, Analysis of the operational behavior and Long–Term performance of a CIS PV system, in: 25th European Photovoltaic Solar Energy Conference and Exhibition (PVSEC) / 5th World Conference on Photovoltaic Energy Conversion (WCPEC), Valencia, Spain, 2010, pp. 3942 – 3946. URL: https://doi.org/10.4229/25thEUPVSEC2010-4DO.11.4.